Altering lipid droplet homeostasis affects *Coxiella burnetii* intracellular growth

Minal Mulye[1+], Brianne Zapata[1,2], and Stacey D. Gilk[1*]

[1] Department of Microbiology and Immunology, Indiana University School of Medicine, Indianapolis, Indiana.

[2] Department of Biology, California State University, Dominguez Hills, Carson, California.

*Corresponding author: 635 Barnhill Rd, MS 420, Indianapolis, IN 46202. Telephone: 317-274-8028. Fax: 317-278-3331. E-mail: sgilk@iupui.edu

+Current address: Marian University College of Osteopathic Medicine, Indianapolis, Indiana.

Running title: Lipid droplets during *Coxiella burnetii* infection.

ABSTRACT

Coxiella burnetii is an obligate intracellular bacterial pathogen and a causative agent of culture-negative endocarditis. While *C. burnetii* initially infects alveolar macrophages, it has also been found in lipid droplet (LD)-containing foamy macrophages in the cardiac valves of endocarditis patients. In addition, transcriptional studies of *C. burnetii*-infected macrophages reported differential regulation of the LD coat protein-encoding gene perilipin 2 *(plin-2)*. To further investigate the relationship between LDs and *C. burnetii*, we compared LD numbers using fluorescence microscopy in mock-infected and *C. burnetii*-infected alveolar macrophages. On average, *C. burnetii*-infected macrophages contained twice as many LDs as mock-infected macrophages. LD numbers increased as early as 24 hours post-infection, an effect reversed by blocking *C. burnetii* protein synthesis. The observed LD accumulation was dependent on the *C. burnetii* Type 4B Secretion System (T4BSS), a major virulence factor that manipulates host cellular processes by secreting bacterial effector proteins into the host cell cytoplasm. To determine the importance of LDs during *C. burnetii* infection, we manipulated LD homeostasis and assessed *C. burnetii* intracellular growth. Surprisingly, blocking LD formation with the pharmacological inhibitors triacsin C or T863, or knocking out acyl-CoA transferase-1 (acat-1) in alveolar macrophages, increased *C. burnetii* growth at least 2-fold. Conversely, preventing LD lipolysis by inhibiting adipose triglyceride lipase (ATGL) with atglistatin almost completely blocked bacterial growth, suggesting LD breakdown is essential for *C. burnetii.* Together these data suggest that maintenance of LD homeostasis, possibly via the *C. burnetii* T4BSS, is critical for bacterial growth.

IMPORTANCE

Host neutral lipid storage organelles known as lipid droplets (LDs) serve as a source of energy, nutrients, and signaling lipids. LDs are associated with infection of the intracellular bacterial pathogen *Coxiella burnetii*, a significant cause of culture-negative endocarditis. While *C. burnetii* was found in LD-rich foamy macrophages in endocarditis patients, little is known about the host LD-*C. burnetii* relationship. We demonstrated *C. burnetii* Type 4B Secretion System (T4BSS)-dependent LD accumulation in macrophages, suggesting a T4BSS-mediated regulation of host LD homeostasis. Further, manipulating LD homeostasis significantly affected bacterial growth, indicating LDs play an important role during *C. burnetii* infection. As *C. burnetii* endocarditis has a 19% mortality rate even in treated patients, exploring the LD-*C. burnetii* association might identify novel therapeutic targets.

INTRODUCTION

Lipid droplets (LDs) are dynamic cytoplasmic organelles which store cellular lipids in eukaryotic cells. LDs are uniquely comprised of a phospholipid monolayer surrounding a hydrophobic core of neutral lipids, primarily sterol esters and triacylglycerols (TAGs). LD assembly begins with neutral lipid synthesis, where fatty acyl CoA synthetases generate long chain fatty acids which are converted to sterol esters and triacyglycerols by acyl-CoA:cholesterol acyltransferase (ACAT) and acyl-CoA:diacylglycerol acyltransferase (DGAT), respectively. Progressive accumulation of neutral lipids in the ER leads to budding of the lipid ester globule surrounded by the ER membrane cytoplasmic leaflet, thus forming LDs (1, 2). Inversely, adipose triglyceride lipase (ATGL) (3) and hormone sensitive lipase (HSL) (4) mediate LD breakdown and release of free cholesterol and fatty acids. Functionally, LDs serve as intracellular lipid

62 reservoirs for membrane synthesis or energy metabolism. In addition, LDs are linked to a range
63 of cellular functions including protein storage, protein degradation and signaling (2, 5).

64 LDs are emerging as important players during host-pathogen interactions. During
65 infection of host cells, Hepatitis C virus (HCV) (6) and Dengue virus (7) co-opt LDs as
66 platforms for viral assembly and replication. Even though blocking LD formation attenuates
67 HCV and Dengue virus replication *in vitro*, the importance of LDs during viral infection still
68 remains elusive (8). LD numbers increased in host cells during infection with several pathogens
69 including HCV (6) and Dengue virus (7), as well as the protozoan parasites *Trypanosoma cruzi*
70 (9), *Plasmodium berghei* (10), *Toxoplasma gondii* (11), *Leishmania amazonensis* (12) and
71 *Leishmania major* (13). In addition, infection with the intracellular bacterial pathogens
72 *Chlamydia* spp. (14), *Mycobacterium* spp. (15-18), *Orientia tsutugamushi* (19), and *Salmonella*
73 *typhimurium* (20) also led to increased LD numbers. Since fatty acids released from host TAGs
74 and sterols can serve as carbon sources during infection (21), *C. trachomatis* (14, 22) and *M.*
75 *tuberculosis* (15) are proposed to use LD components as a major source of energy and nutrients.
76 Furthermore, in cells infected with *M. leprae* (23), *M. bovis* (16), *T. cruzi* (24), and *Leishmania*
77 *infantum chagasi* (25), LDs serve as a source of prostaglandin and leukotriene eicosanoids,
78 important signaling lipids which modulate inflammation and the immune response. These LD-
79 derived eicosanoids potentially favor intracellular pathogen survival by downregulating the
80 immune response (26).

81 LDs have been implicated during infection by *Coxiella burnetii*, a gram-negative
82 intracellular bacterium and the causative agent of human Q fever. Primarily spread through
83 aerosols, *C. burnetii* acute infection is characterized by a debilitating flu-like illness, while
84 chronic disease results in endocarditis. Although *in vitro* and *in vivo C. burnetii* can infect a wide

85 range of cells including epithelial cells and fibroblasts, the bacterium first infects alveolar
86 macrophages during natural infection. Inside the host cell, *C. burnetii* directs formation of a
87 specialized lysosome-like compartment called the parasitophorous vacuole (PV) which is
88 essential for *C. burnetii* survival. PV biogenesis requires the *C. burnetii* type 4B secretion system
89 (T4BSS), which secretes effector proteins into the host cell cytoplasm where they manipulate a
90 wide range of cellular processes. While not established to be T4BSS-dependent, *C. burnetii* is
91 thought to manipulate LDs and other components of host cell lipid metabolism (27-30). *C.*
92 *burnetii*-containing LD-filled foam cells were found in heart valves of an infected patient (31),
93 and LDs were observed in the *C. burnetii* PV lumen of infected human alveolar macrophages
94 (32). Further, two separate microarray analyses reported differential regulation of the LD coat
95 protein *plin-2* in *C. burnetii*-infected human macrophage-like cells (THP-1) (29, 30), suggesting
96 *C. burnetii* induced changes in host cell LDs. Intriguingly, siRNA depletion of the phospholipase
97 involved in LD breakdown, PNPLA2 (also known as ATGL), increased the number of *C.*
98 *burnetii* PVs in HeLa epithelial cells (33). In addition, treatment of monkey kidney epithelial
99 cells (Vero cells) with a broad spectrum antiviral molecule ST699 which localizes to host cell
100 LDs inhibited *C. burnetii* intracellular growth (34). Despite these observations, the importance of
101 LDs during *C. burnetii* infection is not known. In this study, we further examined the
102 relationship between host LDs and *C. burnetii*. We observed a T4BSS-dependent increase in LD
103 numbers in infected mouse alveolar and human monocyte-derived macrophage cell lines.
104 Furthermore, manipulation of LD homeostasis significantly altered *C. burnetii* intracellular
105 growth, thus strongly indicating that LDs play an important role during *C. burnetii* infection.
106
107 **RESULTS**

108 **LD-associated genes are upregulated in *C. burnetii*-infected alveolar macrophages.**

109 To examine the role of LDs in *C. burnetii* pathogenesis, we first analyzed the expression of LD
110 homeostasis-related genes in infected cells. As *C. burnetii* preferentially infects alveolar
111 macrophages during natural infection, we utilized a mouse alveolar macrophage cell line (MH-S)
112 previously established as a model for *C. burnetii* infection (35). Compared to mock-infected cells
113 at day 1 post-infection, *C. burnetii* infection upregulated the expression of genes *acat-1*, *acat-2*
114 and *fabp-4* by more than 1.2 fold (Figure 1). ACATs (acyl coA transferases) catalyze the
115 formation of sterol esters, while FABP-4 (fatty acid binding protein-4) facilitates fatty acid
116 transport for storage in LDs (36). Upregulation of LD-associated genes suggests LDs may
117 increase during *C. burnetii* infection.

118

119 ***C. burnetii* infection results in bacterial protein synthesis-dependent host cell LD**
120 **accumulation.**

121 Previously, at 36 and 72 hours post-infection two separate microarray analyses of *C.*
122 *burnetii*-infected THP-1 cells reported upregulation of the LD coat protein-encoding gene *plin-2*
123 (29, 30). Mahapatra et al. also reported upregulation of *fabp-4* (29). Together with our gene
124 expression analysis, this suggests LD formation may be altered during *C. burnetii* infection. To
125 test this possibility, we stained LDs for the coat protein PLIN2 and quantitated LD numbers per
126 cell in *C. burnetii*-infected cells by fluorescence microscopy. On an average, mock-infected had
127 less than 50 LDs per cell during a 4 day experiment, irrespective of the time point (Figure 2A).
128 In contrast, we observed a significant increase in LDs in infected cells, with an average of more
129 than 90 LDs/cell at 1, 2 and 4 days after *C. burnetii* infection (Figure 2A, gray circles). Notably,
130 LD accumulation occurred as early as 1 day post-infection, when the PV has not expanded and

131 the bacteria are not in log growth (Figure 2D-E). To determine the role of *C. burnetii* in host cell
132 LD accumulation, we blocked bacterial protein synthesis with chloramphenicol (29) and
133 quantitated LD numbers at indicated times. Chloramphenicol-treated *C. burnetii*-infected cells
134 contained 50 or less LDs per cell similar to mock-infected cells (Figure 2B and G). This result
135 suggests *C. burnetii* protein synthesis is required for LD accumulation.
136
137 **Host cell LD accumulation is dependent on the *C. burnetii* Type 4B Secretion System**
138 **(T4BSS).**
139 *C. burnetii* manipulates the host cell by secreting bacterial effector proteins through the
140 T4BSS into the host cytoplasm. To further decipher *C. burnetii's* role in LD accumulation, we
141 analyzed LD numbers at 1, 2, and 4 days after infection with a *C. burnetii* T4BSS *dotA* mutant
142 (37). While the wild-type *C. burnetii*-infected cells had more than 90 LDs per cell (Figure 2A,
143 closed circles; Figure 2E), T4BSS-mutant infected cells contained an average of 50 LDs, similar
144 to mock-infected cells (Figure 2A, triangles; Figure 2F). This suggests the LD accumulation in
145 *C. burnetii*-infected alveolar macrophages involves the *C. burnetii* T4BSS.
146 To confirm the T4BSS-dependent increase in LD accumulation, we analyzed LD
147 numbers in human macrophage-like cells (THP-1). When compared to mock- or T4BSS mutant-
148 infected cells, wild-type *C. burnetii*-infected THP-1 cells had increased LD numbers at 1 and 4
149 days post-infection (Figure 2C), similar to mouse alveolar macrophages. Interestingly, we did
150 not observe T4BSS-dependent LD accumulation at 2 days post-infection. Overall these results
151 demonstrate that *C. burnetii* induces LD accumulation in human and mouse macrophages
152 through a T4BSS-dependent process.
153

154 **Blocking LD formation increases *C. burnetii* growth.**

155 Given our finding that *C. burnetii* appears to actively manipulate host LDs through the
156 T4BSS, we next assessed the importance of LDs during *C. burnetii* infection. We first blocked
157 LD formation using triacsin C, a long chain fatty acyl CoA synthetase inhibitor (38). Compared
158 to vehicle control, triacsin C significantly reduced macrophage LDs, with <5 LDs per cell
159 (Figure 3A-B). We next treated macrophages with triacsin C during *C. burnetii* infection, and
160 quantitated bacterial growth using a fluorescent infectious focus-forming unit (FFU) assay. At
161 various times post-infection, we recovered bacteria from MH-S cells, replated bacteria onto a
162 monolayer of Vero cells, and incubated for 5 days. After staining for *C. burnetii*, we counted the
163 number of fluorescent foci, with 1 focus unit equivalent to 1 viable bacterium. Surprisingly,
164 compared to vehicle-treated cells, triacsin C treatment increased *C. burnetii* growth 5-fold at 4
165 days post-infection (Figure 3F).

166 To further confirm this finding, we used CRISPR/Cas-9 to knockout *acat-1* (Figure 3G),
167 a gene functionally responsible for sterol esterification in macrophages (39) and upregulated in
168 *C. burnetii*-infected cells (Figure 1). While *acat-1*$^{-/-}$ LDs lack sterol esters, fluorescence
169 microscopy revealed similar number of LDs in wild-type and *acat-1*$^{-/-}$ cells (Figure 3A,C).
170 Compared to wild-type cells, *C. burnetii* growth in *acat-1*$^{-/-}$ cells increased 2-fold at 4 days post-
171 infection (Figure 3H), indicating that blocking sterol esterification favors *C. burnetii* growth. To
172 further deplete both TAG- and sterol ester-containing LDs, we treated *acat-1*$^{-/-}$ cells with the
173 DGAT-1 inhibitor T863, which specifically blocks formation of TAGs (40). T863 treatment
174 significantly reduced LDs in *acat-1*$^{-/-}$ macrophages, compared to untreated wild-type or *acat-1*$^{-/-}$
175 macrophages (Figure 3A, C, D). *C. burnetii* growth increased 2-fold in T863-treated *acat-1*$^{-/-}$
176 cells compared to vehicle-treated *acat-1*$^{-/-}$ cells (Figure 3I), demonstrating that blocking both

177 TAG- and sterol ester-containing LDs improves *C. burnetii* growth.

178

179 **Inhibiting LD breakdown blocks *C. burnetii* growth.**

180 Because blocking LD formation appeared to benefit *C. burnetii,* we next examined *C.*
181 *burnetii* growth after inhibiting LD breakdown. When cells or tissues require fatty acids or
182 cholesterol, cytosolic lipases, including adipose triglyceride lipase (ATGL) (3) and hormone
183 sensitive lipase (HSL) (2, 4), hydrolyze TAGs and sterol esters stored in LDs. ATGL catalyzes
184 the initial step of lipolysis converting TAGs to DAGs whereas HSL hydrolyses DAGs to MAGs
185 (41). To block LD breakdown, we first inhibited HSL with a selective inhibitor CAY10499 (42).
186 HSL inhibitor-treated cells showed no significant difference in *C. burnetii* growth compared to
187 vehicle-treated cells (Figure 4A) suggesting conversion of DAGs to MAGs is not important for
188 bacterial intracellular growth.

189 To further study the importance of LD breakdown, we inhibited ATGL with the selective
190 and competitive inhibitor atglistatin, which binds the ATGL patatin-like phospholipase domain
191 (43). To eliminate the possibility of ATGL inhibiting a *C. burnetii* phospholipase, we first
192 measured viability of axenic *C. burnetii* cultures in the presence or absence of atglistatin (Figure
193 4B). Treatment for 4 days had no effect on axenic bacterial growth, indicating atglistatin does
194 not directly affect *C. burnetii*.

195 We next tested the effect of atglistatin on intracellular bacteria. After atglistatin treatment
196 of wild-type MH-S cells, we observed larger LDs, although the number did not significantly
197 increase (Figure 3E). Interestingly, *C. burnetii* intracellular growth in atglistatin-treated wild-
198 type MH-S cells decreased 5-fold, with essentially no growth (Figure 4C). Further, atglistatin-
199 treated *acat-1*$^{-/-}$ cells, which contain TAG-rich LDs, also showed reduced bacterial growth

200 (Figure 4D) suggesting TAG hydrolysis to DAG is critical to support *C. burnetii* growth.
201 Together, these data demonstrate that blocking LD breakdown, particularly TAG to DAG
202 conversion significantly inhibits intracellular *C. burnetii* growth.
203

204 **DISCUSSION**

205 Several intracellular pathogens intercept host cell LDs to promote their growth. While
206 certain viruses utilize LDs as platforms for assembly, many bacteria and parasites facilitate
207 intracellular growth by exploiting LDs for nutrition. To understand the role of LDs during *C.*
208 *burnetii* infection, we assessed changes in LD numbers in *C. burnetii*-infected cells and
209 determined the effect of manipulating LD homeostasis on bacterial growth. Our studies revealed
210 a bacterial T4BSS-dependent increase in LD numbers in *C. burnetii*-infected macrophages.
211 Further, manipulating LD homeostasis significantly altered *C. burnetii* growth. While blocking
212 LD formation promoted *C. burnetii* growth, inhibiting LD breakdown, particularly hydrolysis of
213 TAGs to DAGs, dramatically decreased bacterial growth. Collectively, our data strongly suggest
214 LDs play an important role during *C. burnetii* intracellular growth.

215 LD formation requires sterol and fatty acid esterification by the enzymes ACAT and
216 DGAT, while LD lipolysis is catalyzed by HSL and ATGL. Once formed, LD maintenance
217 requires the LD-associated proteins PLINs. Previously, two separate microarray analyses
218 reported upregulation of *plin-2* in *C. burnetii*-infected human macrophage-like cells (THP-1)
219 (29, 30), suggesting *C. burnetii* induced changes in host cell LDs. Although we did not observe
220 changes in *plin-2* transcript levels, post-translational regulation of *plin-2* (44) could potentially
221 contribute to changes in LD numbers in infected macrophages. However, consistent with the

222 upregulation of LD-formation genes *acat* and *fabp-4,* our results demonstrated that LD numbers
223 increase in *C. burnetii*-infected mouse and human macrophages.

224 Notably, LD accumulation occurred as early as day 1 post-infection, when the PV has not
225 expanded and the bacteria are not in log growth. This suggests that LD accumulation is not a host
226 response to a large and growing PV but could be in response to bacterial ligands or due to a
227 process actively manipulated by *C. burnetii* itself. Previously, based on microarray analysis of *C.*
228 *burnetii*-infected cells where bacterial protein synthesis was blocked, Mahapatra *et al.* identified
229 36 host cell genes specifically regulated by *C. burnetii* proteins during early stages of infection.
230 These genes were predominantly involved in the innate immune response, cell death and
231 proliferation, vesicular trafficking, cytoskeletal organization and lipid homeostasis. Interestingly,
232 changes in *plin-2* expression level in infected cells was dependent on *C. burnetii* protein
233 synthesis (29) suggesting a role for bacterial proteins in LD accumulation. In agreement with this
234 data, we found that blocking *C. burnetii* protein synthesis prevented increased LD accumulation
235 in mouse alveolar macrophages at all analyzed times post-infection. These data together suggest
236 that *C. burnetii* actively manipulates host LDs at early stages of infection.

237 Beginning 1 hour post-infection in bone marrow-derived macrophages and 8 hours in
238 HeLa cells, *C. burnetii* secretes effector proteins via T4BSS (45) to modulate host cell functions
239 and promote its intracellular survival. Intriguingly, a *C. burnetii* T4BSS mutant did not increase
240 host cell LD numbers, suggesting a T4BSS-dependent increase in LD accumulation during wild-
241 type *C. burnetii* infection. The same result was observed in both mouse and human macrophages,
242 demonstrating that the *C. burnetii*-induced increase in LDs is independent of species and
243 dependent on the *C. burnetii* T4BSS. This finding suggests that one or more T4BSS effector
244 proteins may actively manipulate LDs, possibly by directly targeting proteins involved in LD

245 homeostasis. For example, the *Salmonella* Typhimurium type 3 secretion system (T3SS) effector
246 protein SseJ esterifies cholesterol and increases LD numbers when ectopically expressed in
247 epithelial and macrophage cells (20). The *C. trachomatis* secreted protein Lda3 localizes to the
248 LD surface and is involved in LD translocation into the *Chlamydia*-containing inclusion (22).
249 Thus far, none of the identified *C. burnetii* T4BSS secreted effector proteins localize to host LDs
250 or associate with proteins involved in LD homeostasis. It is also possible that rather than *de novo*
251 formation, increased LD numbers result from fission of preexisting LDs (46). As observed by
252 microscopy, the LD size in *C. burnetii*-infected macrophages appeared smaller than the mock- or
253 T4BSS mutant-infected macrophages. Smaller, more numerous LDs might result from *C.*
254 *burnetii* T4BSS-mediated fission of the existing LDs.

255 While *C. burnetii* T4BSS effector proteins might directly target LD homeostasis
256 pathways, LD accumulation may also be a host innate immune response. In other diseases, LD
257 accumulation occurs during the inflammatory response in macrophages in atherosclerotic lesions
258 (47), leukocytes from joints of patients with inflammatory arthritis (48), and eosinophils in
259 allergic inflammation (49). Thus, an innate immune response to the T4BSS apparatus or T4BSS
260 effector proteins may increase LD numbers in *C. burnetii*-infected macrophages. Additionally,
261 bystander response to bacterial components including TLR ligand LPS could result in increased
262 LD accumulation (16, 50). However, T4BSS mutant and protein-synthesis blocked *C. burnetii*
263 have similar surface ligands to wild-type bacterium but show no increase in LD accumulation
264 thus arguing against the contribution of *C. burnetii* LPS and other surface ligands. Overall, while
265 our data demonstrate that the *C. burnetii* T4BSS is involved in LD accumulation in both mouse
266 and human macrophages, the bacterial effector proteins and the specific LD processes targeted
267 remain unknown.

268 Besides T4BSS-dependent increase in LD accumulation, we found that manipulating LD
269 homeostasis, in particular fatty acids, significantly altered *C. burnetii* growth. Surprisingly,
270 blocking LD formation by pharmaceutical and genetic approaches, which increases the
271 availability of free fatty acids, led to improved *C. burnetii* fitness in macrophages. Conversely,
272 reducing fatty acid availability by inhibiting breakdown of LD-derived TAGs to DAGs blocked
273 *C. burnetii* growth. Intriguingly, DAG to MAG conversion did not affect bacterial growth,
274 suggesting that DAGs in particular are critical for *C. burnetii* infection. DAGs and other fatty
275 acids liberated during LD breakdown can be re-esterified or serve as signaling cofactors,
276 building blocks for membranes, or substrates for β-oxidation (2). Other bacterial pathogens are
277 known to target LDs as a source of lipids. For example, *M. tuberculosis* uses free fatty acids as a
278 source of energy and carbon (15, 51), while *C. trachomatis* is hypothesized to break down
279 bacterial inclusion-associated host LDs to provide lipids for bacterial growth (14). It not known
280 if free fatty acids or sterols liberated from LDs, either in the cytosol or possibly in PV lumen, are
281 used directly by *C. burnetii*.

282 In addition to serving as a source of free fatty acids and sterols, macrophage LDs are rich
283 in substrates and enzymes that generate prostaglandins and leukotrienes, which are arachidonic
284 acid-derived inflammatory lipid mediators (52, 53). In *M. leprae*-infected Schwann cells and *M.*
285 *bovis* BCG-infected macrophages, increased LD biogenesis correlates with increased production
286 of prostaglandin E2 (PGE2), linking LDs to the production of innate immune modulators (17,
287 54). PGE2 has a potential role in inhibiting TH1 responses important in clearance of intracellular
288 pathogens (24) including *C. burnetii* (55). Interestingly, elevated levels of PGE2 were observed
289 in *C. burnetii* endocarditis patients and linked to *C. burnetii*-mediated immunosuppression.
290 Koster *et al.* reported lymphocytes from chronic Q fever patients being unresponsive to *C.*

291 *burnetii* antigens, an effect reversed by PGE2 suppression with indomethacin (56). In addition,
292 after stimulation with *C. burnetii* antigens, monocytes from Q fever patients produced PGE2,
293 which in turn downregulated T lymphocyte-mediated IL-2 and IFNγ production. Interestingly,
294 PGE2 synthesis inhibitor Piroxicam reversed this downregulation of pro-inflammatory cytokine
295 production (57). Thus, while PGE2 appears to play a role in Q fever patients, the relationship
296 between *C. burnetii*-induced LDs and PGE2 production is not known. Considering that LD
297 breakdown can serve multiple functions, *C. burnetii* could use LDs either as a source of nutrients
298 or for production of lipid immune mediators like PGE2, which could then modulate the host cell
299 response to promote *C. burnetii* intracellular growth.

300 In summary, our data demonstrate that LD homeostasis is important for *C. burnetii*
301 intracellular survival. Because the *C. burnetii* T4BSS is involved in LD accumulation,
302 characterizing bacterial T4BSS effector proteins that target host LD homeostasis will help further
303 understand the role of LDs in *C. burnetii* pathogenesis.

304

305 **MATERIALS AND METHODS**

306 Bacteria and mammalian cells

307 *C. burnetii* Nine Mile Phase II (NMII; clone 4, RSA439) were purified from Vero cells (African
308 green monkey kidney epithelial cells, ATCC CCL-81; American Type Culture Collection,
309 Manassas, VA) and stored as previously described (58). For experiments examining T4BSS-
310 dependent accumulation of LDs, NMII and the *dotA* mutant (37) were grown for 4 days in
311 ACCM-2, washed twice with phosphate buffered saline (PBS) and stored as previously described
312 (59). Vero, mouse alveolar macrophages (MH-S; ATCC CRL-2019) and human monocytes
313 (THP-1; ATCC TIB-202) were maintained in RPMI (Roswell Park Memorial Institute) 1640

314 medium (Corning, New York, NY, USA) containing 10% fetal bovine serum (Atlanta
315 Biologicals, Norcross, GA, USA) at 37°C and 5% CO_2 and human embryonic kidney 293
316 (HEK293T; ATCC CRL-3216) in DMEM (Dulbecco's Modified Eagle Medium) (Corning, New
317 York, NY, USA) containing 10% fetal bovine serum at 37°C and 5% CO_2. THP-1 cells were
318 differentiated with 200 nM of phorbol 12-myristate 13-acetate (PMA) for 24 hours. PMA was
319 removed, and the cells rested for 48 hours prior to infection. The multiplicity of infection (MOI)
320 was optimized at 37°C and 5% CO_2 for each bacterial stock, cell type and infection condition for
321 a final infection of ~1 internalized bacterium/cell.
322
323 Generating *acat-1*$^{-/-}$ MH-S cell line
324 The guide RNA sequence 5′TCGCGTCTCCATGGCTGCCC3′ to mouse *acat-1* was selected
325 using the optimized CRISPR design site crispr.mit.edu. Oligonucleotides were synthesized (IDT,
326 Coralville, IA, USA), annealed, and cloned into the lentiCRISPRv2 plasmid (a gift from Feng
327 Zhang, Addgene # 52961, Cambridge, MA, USA) (60), at the BsmBI restriction site to generate
328 plentiCRISPRv2-*acat-1*. To generate lentivirus, HEK293T cells were co-transfected with
329 plentiCRISPRv2-*acat-1* and packaging plasmids pVSVg (Addgene # 8454), pRSV-Rev
330 (Addgene # 12253), and pMDLg/pRRE (Addgene # 12251) using FuGENE6 reagent (Promega,
331 Madison, WI, USA). At 48 hours post-transfection, supernatant was collected, centrifuged at
332 3000xg, and then filtered with 0.45µm filter to remove cells and debris. Supernatant was
333 concentrated using the Lenti-X concentrator (Catalog # PT4421-2, Clontech, USA) and viral
334 RNA isolated using Viral RNA isolation kit (Catalog # 740956, Macherey-Nagel, Germany) to
335 determine viral titer using Lenti-X qRT-PCR titration kit (Catalog # PT4006-2, Clontech). Viral
336 titers were optimized for transduction of MH-S cells to generate stable *acat-1*$^{-/-}$ cells.

337 $2x10^5$ MH-S cells were plated in a 6 well plate and transduced with 5.8 x 10^6 viral
338 particles/ml. 1 µg/ml puromycin was used for selection 48 hours post-transduction and continued
339 for 24 hours. The puromycin was then removed and the cells allowed to recover before isolating
340 individual clones by limiting dilution.

341 To confirm disruption of *acat-1*, clones were lysed in 2% SDS (Sigma-Aldrich, St. Louis,
342 MO, USA) for SDS-PAGE and immunoblotting with 1:1000 rabbit anti-mouse ACAT1-specific
343 antibody (Catalog # NBP189285, Novus Biologicals, Littleton, CO, USA) and 1:4000 GAPDH
344 loading control monoclonal antibody (Catalog # MA5-15738, ThermoFisher Scientific,
345 Waltham, MA, USA).

346

347 Gene expression analysis of LD genes

348 $2x10^5$ MH-S cells were infected in a 6 well plate. At day 1 post-infection, host cell RNA was
349 isolated using RNEasy mini kit (Catalog # 74104, Qiagen) and reverse transcribed to cDNA
350 using Superscript first strand synthesis system (Catalog # 11904-018, Invitrogen). Gene
351 expression analysis was performed using TaqMan array mouse lipid regulated genes (Catalog #
352 4415461, Applied Biosystems). Fold change was calculated compared to mock-infected cells in
353 6 independent experiments.

354

355 LD quantitation

356 $1x10^5$ MH-S cells were plated onto ibidi-treated channel µslide $VI^{0.4}$ ($3x10^3$ cells per channel;
357 Ibidi, Verona, WI) and allowed to adhere overnight. After infecting with *C. burnetii* for 1 hour,
358 cells were gently washed with phosphate buffered saline (PBS) to remove extracellular bacteria,
359 and incubated in 10% FBS-RPMI. For blocking bacterial protein synthesis, infected cells were

360 incubated with 3 μg/ml chloramphenicol containing 10% FBS-RPMI for the remainder of
361 experiment, replenishing media every 24 hours. At different times post-infection, infected cells
362 were fixed with 2.5% paraformaldehyde on ice for 15 min, then permeabilized/blocked for 15
363 min with 0.1% saponin and 1% bovine serum albumin (BSA) in PBS (saponin-BSA-PBS) and
364 stained with 1:1000 rabbit anti-mouse PLIN2 primary antibody (Catalog # PA1-16972,
365 ThermoFisher Scientific), 1:2000 guinea-pig anti-*C. burnetii* primary antibody (61) and 1:1000
366 rat anti-LAMP (Catalog # 553792, BD Biosciences) primary antibody in saponin-BSA-PBS for 1
367 hour. THP-1 cells were stained with 1:500 guinea-pig anti-human PLIN2 primary antibody
368 (Catalog # 20R-AP002, Fitzgerald Industries International, Acton, MA), 1:2000 rabbit anti-*C.*
369 *burnetii* primary antibody and 1:1000 rat anti-LAMP primary antibody in saponin-BSA-PBS for
370 1 hour. After three washes with PBS, cells were stained with 1:2000 AlexaFluor 488 anti-rabbit,
371 AlexaFluor 594 anti-guinea pig and AlexaFluor 647 anti-rat secondary antibodies (Invitrogen)
372 for 1 hour. ProLong Gold mount (Invitrogen) was added to the wells after washing with PBS and
373 slides visualized on a Leica inverted DMI6000B microscope (100X oil). The number of LDs per
374 cell was quantitated for 25 cells per condition in duplicate in each of three individual
375 experiments, with only bacteria-containing cells counted for *C. burnetii*-infected cells.
376
377 <u>Inhibitors</u>
378 Each LD homeostasis inhibitor used was diluted in DMSO based on manufacturer's instructions
379 and optimum inhibitor concentration was determined based on 100% host cell viability
380 determined by trypan blue staining, and changes in LD numbers per cell. The optimum
381 concentrations determined for each inhibitor was: Triacsin C (Enzo Life Sciences, Farmingdale,

382 NY, USA) – 10 μM, T863 (Sigma-Aldrich) – 10 μM, CAY10499 (Cayman Chemicals, Ann
383 Arbor, MI, USA) - 10 μM, Atglistatin (Cayman Chemicals) – 20 μM.
384
385 <u>*C. burnetii* growth by fluorescent infectious focus-forming unit (FFU) assay.</u>
386 To measure growth of *C. burnetii* in wild-type and *acat-1*$^{-/-}$ MH-S cells, 5x10^{4} cells/well were
387 infected for 1 hour in a 48 well plate, washed with PBS, and then incubated with media
388 containing respective vehicle and inhibitors. At the indicated time points, the media was
389 removed and cells were incubated with sterile water for 5 min, pipetted up and down and the
390 lysate diluted 1:5 in 2% FBS-RPMI. Serial dilutions were added to 24 well plate containing
391 confluent monolayers of Vero cells, incubated for 5 days, fixed with methanol and stained with
392 rabbit anti-*C. burnetii* antibody as well as DAPI to confirm monolayer integrity. Four fields per
393 well were captured on an Evos automated microscope (ThermoFisher) with 4X objective and
394 fluorescent foci units were quantitated using ImageJ. Each experiment was done in duplicate.
395
396 <u>Atglistatin-treatment of *C. burnetii* axenic cultures</u>
397 To test bacterial sensitivity to atglistatin, ACCM-2 was inoculated at approximately 1x10^{5}
398 bacteria/ml with *C. burnetii* NMII and grown for 3 days as previously described (59). Bacteria
399 (500 μl) were then incubated with DMSO or atglistatin in 24 well plates under normal *C.*
400 *burnetii* culture conditions. Media was replenished every 24 hours by centrifuging the
401 supernatant at 20000xg for 10 min, and bacterial pellet resuspended in new media containing
402 inhibitor. After 4 days, bacteria were diluted 1:10 in 2% FBS-RPMI and serial dilutions were
403 added to confluent Vero cell monolayers in a 96 well ibidi-treated μplate. At 5 days post-

404 infection, the plate was stained and fluorescent foci were determined as above. Each experiment
405 was done in duplicate.
406
407 Statistical analysis
408 Statistical analyses were performed using two-tailed paired t-test, ordinary one-way ANOVA or
409 two-way ANOVA with Tukey's or Bonferroni's multiple comparisons test in Prism (GraphPad
410 Software, Inc., La Jolla, CA).
411
412 **FIGURE LEGENDS:**
413 **Figure 1: LD-associated genes are upregulated in *C. burnetii*-infected alveolar**
414 **macrophages.**

415 MH-S macrophages were infected with wild-type *C. burnetii* and RNA was collected at day 1
416 post-infection. Gene expression analysis was performed using Applied Biosystems lipid-
417 regulated TaqMan Array. Fold change was calculated compared to mock-infected samples. Error
418 bars show the mean of 6 independent experiments +/- SEM * =p<0.05, *** =p <0.001 compared
419 to respective mock-infected cells as determined by two-tailed paired t-test.

420 **Figure 2: *C. burnetii* infection leads to host cell LD accumulation and is dependent on**
421 **bacterial protein synthesis and the T4BSS.**

422 Macrophages were infected with *C. burnetii* and at different times post-infection, cells were
423 stained for PLIN2 (LDs; green), *C. burnetii* (red) and nucleus (blue). LD number per cell were
424 quantitated by fluorescence microscopy.

425 A) LD numbers in wild-type *C. burnetii* and *dotA* mutant- infected MH-S macrophages.

426 B) LD numbers in MH-S macrophages infected with wild-type *C. burnetii* and treated with
427 chloramphenicol (3µg/ml).

428 C) LD numbers in wild-type *C. burnetii* and *dotA* mutant- infected THP-1 macrophage-like cells.

429 D) Images of LDs and bacteria in MH-S cells at day 1 post-infection imaged at 100X. Scale bar
430 = 10 µm. Error bars show the mean of 3 independent experiments +/- SEM * =p<0.05, ** =p
431 <0.01, *** =p <0.001 as determined by ordinary one-way ANOVA with Tukey post-hoc test.

432

433 **Figure 3: Blocking LD formation increases *C. burnetii* growth.**

434 Wild-type *C. burnetii* growth in infected MH-S cells treated with different inhibitors was
435 measured at 2 and 4 days post-infection by FFU assay.

436 A-E) Representative images for wild-type MH-S macrophages treated with inhibitors, fixed,
437 stained for PLIN2 (LDs; green) and *C. burnetii* (red) and imaged day 4 post-treatment at 100X.
438 Scale bar = 10 µm.

439 F) Growth while inhibiting LD formation with triacsin C (10 µM) in wild-type MH-S
440 macrophages. Error bars represent the mean of 4 independent experiments +/- SEM. **= p <0.01
441 compared to vehicle-treated cells as determined by two-way ANOVA with Bonferroni post-hoc
442 test.

443 G) ACAT1 protein expression in wild-type and *acat-1*$^{-/-}$ macrophages. Cell lysates were
444 immunoblotted and ACAT1 protein levels were compared with GAPDH as loading control.

445 H) *C. burnetii* growth in vehicle-treated wild-type and *acat-1*$^{-/-}$ MH-S macrophages and (I) T863-
446 treated *acat-1*$^{-/-}$ MH-S macrophages. Error bars represent the mean of at least 3 independent

447 experiments +/- SEM., * =p<0.05, *** =p <0.001 as determined by two-way ANOVA with
448 Bonferroni post-hoc test.

449

450 **Figure 4: Inhibiting LD breakdown blocks *C. burnetii* growth.**

451 Effect of HSL inhibitor CAY10499 and ATGL inhibitor atglistatin on viability of axenic and
452 intracellular wild-type *C. burnetii* was determined by FFU assay.

453 A) *C. burnetii* growth in CAY10499-treated (10 μM) and vehicle-treated wild-type MH-S
454 macrophages. Error bars represent the mean of 3 independent experiments +/- SEM. ns = not
455 significant compared to vehicle-treated cells as determined by two-way ANOVA with
456 Bonferroni post-hoc test.

457 B) Direct effect of atglistatin on wild-type *C. burnetii*. Atglistatin was added to axenic *C.*
458 *burnetii* cultures and bacterial viability was determined at day 4 using FFU assay. Error bars
459 represent the mean of 3 independent experiments +/- SEM. ns = not significant compared to
460 vehicle treatment as determined by ordinary one -way ANOVA with Tukey post-hoc test.

461 C) *C. burnetii* growth in atglistatin-treated (20 μM) and vehicle-treated wild-type MH-S
462 macrophages. Error bars represent the mean of 4 independent experiments +/- SEM. *= p <0.05,
463 ****= p <0.0001 compared to vehicle-treated cells as determined by two-way ANOVA with
464 Bonferroni post-hoc test.

465 D) *C. burnetii* growth in atglistatin-treated (20 μM) and vehicle-treated *acat-1*$^{-/-}$ MH-S
466 macrophages. Error bars represent the mean of 4 independent experiments +/- SEM. **= p <0.01
467 compared to vehicle-treated cells as determined by two-way ANOVA with Bonferroni post-hoc
468 test.

ACKNOWLEDGMENTS

This research was supported by National Institutes of Health (AI21786; S.D.G.), American Heart Association (16POST27250157; M.M.) and National Institutes of Health (5R25GM07592; B.Z.). We thank Anna Justis, Tatiana Clemente and Rajshekar Gaji for critical reading of the manuscript and members of the IU Biology of Intracellular Pathogens Group for helpful suggestions.

We have no conflicts of interest to declare.

REFERENCES

1. **Pol A, Gross SP, Parton RG.** 2014. Review: biogenesis of the multifunctional lipid droplet: lipids, proteins, and sites. The Journal of Cell Biology **204:**635-646.
2. **Walther TC, Farese RV, Jr.** 2012. Lipid droplets and cellular lipid metabolism. Annual Review of Biochemistry **81:**687-714.
3. **Haemmerle G, Lass A, Zimmermann R, Gorkiewicz G, Meyer C, Rozman J, Heldmaier G, Maier R, Theussl C, Eder S, Kratky D, Wagner EF, Klingenspor M, Hoefler G, Zechner R.** 2006. Defective lipolysis and altered energy metabolism in mice lacking adipose triglyceride lipase. Science **312:**734-737.
4. **Vaughan M, Berger JE, Steinberg D.** 1964. Hormone-Sensitive Lipase and Monoglyceride Lipase Activities in Adipose Tissue. The Journal of biological chemistry **239:**401-409.
5. **Welte MA.** 2007. Proteins under new management: lipid droplets deliver. Trends in cell biology **17:**363-369.
6. **Filipe A, McLauchlan J.** 2015. Hepatitis C virus and lipid droplets: finding a niche. Trends in Molecular Medicine **21:**34-42.
7. **Samsa MM, Mondotte JA, Iglesias NG, Assuncao-Miranda I, Barbosa-Lima G, Da Poian AT, Bozza PT, Gamarnik AV.** 2009. Dengue virus capsid protein usurps lipid droplets for viral particle formation. PLoS Pathogens **5:**e1000632.
8. **Herker E, Ott M.** 2012. Emerging role of lipid droplets in host/pathogen interactions. Journal of Biological Chemistry **287:**2280-2287.
9. **D'Avila H, Freire-de-Lima CG, Roque NR, Teixeira L, Barja-Fidalgo C, Silva AR, Melo RC, Dosreis GA, Castro-Faria-Neto HC, Bozza PT.** 2011. Host cell lipid bodies triggered by *Trypanosoma cruzi* infection and enhanced by the uptake of apoptotic cells are associated with prostaglandin E(2) generation and increased parasite growth. Journal of Infectious Disease **204:**951-961.

505 10. **Pulido-Mendez M, Finol HJ, Giron ME, Aguilar I.** 2006. Ultrastructural pathological
506 changes in mice kidney caused by *Plasmodium berghei* infection. Journal of
507 submicroscopic cytology and pathology **38:**143-148.
508 11. **Charron AJ, Sibley LD.** 2002. Host cells: mobilizable lipid resources for the
509 intracellular parasite *Toxoplasma gondii*. Journal of cell science **115:**3049-3059.
510 12. **Lecoeur H, Giraud E, Prevost MC, Milon G, Lang T.** 2013. Reprogramming neutral
511 lipid metabolism in mouse dendritic leucocytes hosting live *Leishmania amazonensis*
512 amastigotes. PLoS neglected tropical diseases **7:**e2276.
513 13. **Rabhi S, Rabhi I, Trentin B, Piquemal D, Regnault B, Goyard S, Lang T,**
514 **Descoteaux A, Enninga J, Guizani-Tabbane L.** 2016. Lipid Droplet Formation, Their
515 Localization and Dynamics during *Leishmania major* Macrophage Infection. PLoS One
516 **11:**e0148640.
517 14. **Kumar Y, Cocchiaro J, Valdivia RH.** 2006. The obligate intracellular pathogen
518 *Chlamydia trachomatis* targets host lipid droplets. Current biology **16:**1646-1651.
519 15. **Daniel J, Maamar H, Deb C, Sirakova TD, Kolattukudy PE.** 2011. *Mycobacterium*
520 *tuberculosis* uses host triacylglycerol to accumulate lipid droplets and acquires a
521 dormancy-like phenotype in lipid-loaded macrophages. PLoS Pathogens **7:**e1002093.
522 16. **D'Avila H, Melo RC, Parreira GG, Werneck-Barroso E, Castro-Faria-Neto HC,**
523 **Bozza PT.** 2006. *Mycobacterium bovis* bacillus Calmette-Guerin induces TLR2-mediated
524 formation of lipid bodies: intracellular domains for eicosanoid synthesis in vivo. Journal
525 of Immunology **176:**3087-3097.
526 17. **D'Avila H, Roque NR, Cardoso RM, Castro-Faria-Neto HC, Melo RC, Bozza PT.**
527 2008. Neutrophils recruited to the site of *Mycobacterium bovis* BCG infection undergo
528 apoptosis and modulate lipid body biogenesis and prostaglandin E production by
529 macrophages. Cellular microbiology **10:**2589-2604.
530 18. **Mattos KA, Lara FA, Oliveira VG, Rodrigues LS, D'Avila H, Melo RC, Manso PP,**
531 **Sarno EN, Bozza PT, Pessolani MC.** 2011. Modulation of lipid droplets by
532 *Mycobacterium leprae* in Schwann cells: a putative mechanism for host lipid acquisition
533 and bacterial survival in phagosomes. Cellular microbiology **13:**259-273.
534 19. **Ogawa M, Fukasawa M, Satoh M, Hanada K, Saijo M, Uchiyama T, Ando S.** 2014.
535 The intracellular pathogen *Orientia tsutsugamushi* responsible for scrub typhus induces
536 lipid droplet formation in mouse fibroblasts. Microbes and Infection **16:**962-966.
537 20. **Nawabi P, Catron DM, Haldar K.** 2008. Esterification of cholesterol by a type III
538 secretion effector during intracellular Salmonella infection. Molecular microbiology
539 **68:**173-185.
540 21. **Barisch C, Soldati T.** 2017. Breaking fat! How mycobacteria and other intracellular
541 pathogens manipulate host lipid droplets. Biochimie **141:**54-61.
542 22. **Cocchiaro JL, Kumar Y, Fischer ER, Hackstadt T, Valdivia RH.** 2008. Cytoplasmic
543 lipid droplets are translocated into the lumen of the *Chlamydia trachomatis*
544 parasitophorous vacuole. Proceedings of the National Academy of Sciences of the U S A
545 **105:**9379-9384.
546 23. **Mattos KA, D'Avila H, Rodrigues LS, Oliveira VG, Sarno EN, Atella GC, Pereira**
547 **GM, Bozza PT, Pessolani MC.** 2010. Lipid droplet formation in leprosy: Toll-like
548 receptor-regulated organelles involved in eicosanoid formation and *Mycobacterium*
549 *leprae* pathogenesis. Journal of leukocyte biology **87:**371-384.

550 24. **Toledo DA, Roque NR, Teixeira L, Milan-Garces EA, Carneiro AB, Almeida MR,**
551 **Andrade GF, Martins JS, Pinho RR, Freire-de-Lima CG, Bozza PT, D'Avila H,**
552 **Melo RC.** 2016. Lipid Body Organelles within the Parasite *Trypanosoma cruzi*: A Role
553 for Intracellular Arachidonic Acid Metabolism. PLoS One **11:**e0160433.
554 25. **Araujo-Santos T, Rodriguez NE, Moura-Pontes S, Dixt UG, Abanades DR, Bozza**
555 **PT, Wilson ME, Borges VM.** 2014. Role of prostaglandin F2alpha production in lipid
556 bodies from *Leishmania infantum chagasi*: insights on virulence. Journal of Infectious
557 Disease **210:**1951-1961.
558 26. **Melo RC, Weller PF.** 2016. Lipid droplets in leukocytes: Organelles linked to
559 inflammatory responses. Experimental cell research **340:**193-197.
560 27. **Justis AV, Hansen B, Beare PA, King KB, Heinzen RA, Gilk SD.** 2016. Interactions
561 between the *Coxiella burnetii* parasitophorous vacuole and the endoplasmic reticulum
562 involve the host protein ORP1L. Cellular Microbiology doi:10.1111/cmi.12637.
563 28. **Martinez E, Allombert J, Cantet F, Lakhani A, Yandrapalli N, Neyret A, Norville**
564 **IH, Favard C, Muriaux D, Bonazzi M.** 2016. *Coxiella burnetii* effector CvpB
565 modulates phosphoinositide metabolism for optimal vacuole development. Proceedings
566 of the National Academy of Sciences of the United States of America **113:**E3260-3269.
567 29. **Mahapatra S, Ayoubi P, Shaw EI.** 2010. *Coxiella burnetii* Nine Mile II proteins
568 modulate gene expression of monocytic host cells during infection. BMC Microbiology
569 **10:**244.
570 30. **Ren Q, Robertson SJ, Howe D, Barrows LF, Heinzen RA.** 2003. Comparative DNA
571 microarray analysis of host cell transcriptional responses to infection by *Coxiella burnetii*
572 or *Chlamydia trachomatis*. Annals of the New York Academy of Sciences **990:**701-713.
573 31. **Brouqui P, Dumler JS, Raoult D.** 1994. Immunohistologic demonstration of *Coxiella*
574 *burnetii* in the valves of patients with Q fever endocarditis. The American journal of
575 medicine **97:**451-458.
576 32. **Graham JG, MacDonald LJ, Hussain SK, Sharma UM, Kurten RC, Voth DE.** 2013.
577 Virulent *Coxiella burnetii* pathotypes productively infect primary human alveolar
578 macrophages. Cellular Microbiology **15:**1012-1025.
579 33. **McDonough JA, Newton HJ, Klum S, Swiss R, Agaisse H, Roy CR.** 2013. Host
580 pathways important for *Coxiella burnetii* infection revealed by genome-wide RNA
581 interference screening. mBio **4:**e00606-00612.
582 34. **Sandoz KM, Valiant WG, Eriksen SG, Hruby DE, Allen RD, 3rd, Rockey DD.** 2014.
583 The broad-spectrum antiviral compound ST-669 restricts chlamydial inclusion
584 development and bacterial growth and localizes to host cell lipid droplets within treated
585 cells. Antimicrobial agents and chemotherapy **58:**3860-3866.
586 35. **Soltysiak KA, van Schaik EJ, Samuel JE.** 2015. Surfactant protein D binds to *Coxiella*
587 *burnetii* and results in a decrease in interactions with murine alveolar macrophages. PLoS
588 One **10:**e0136699.
589 36. **Storch J, Thumser AE.** 2000. The fatty acid transport function of fatty acid-binding
590 proteins. Biochimica et biophysica acta **1486:**28-44.
591 37. **Beare PA, Gilk SD, Larson CL, Hill J, Stead CM, Omsland A, Cockrell DC, Howe**
592 **D, Voth DE, Heinzen RA.** 2011. Dot/Icm type IVB secretion system requirements for
593 *Coxiella burnetii* growth in human macrophages. mBio **2:**e00175-00111.
594 38. **Igal RA, Wang P, Coleman RA.** 1997. Triacsin C blocks *de novo* synthesis of
595 glycerolipids and cholesterol esters but not recycling of fatty acid into phospholipid:

596 evidence for functionally separate pools of acyl-CoA. The Biochemical journal **324 (Pt**
597 **2):**529-534.
598 39. **Rudel LL, Lee RG, Cockman TL.** 2001. Acyl coenzyme A: cholesterol acyltransferase
599 types 1 and 2: structure and function in atherosclerosis. Current opinion in lipidology
600 **12:**121-127.
601 40. **Cao J, Zhou Y, Peng H, Huang X, Stahler S, Suri V, Qadri A, Gareski T, Jones J,**
602 **Hahm S, Perreault M, McKew J, Shi M, Xu X, Tobin JF, Gimeno RE.** 2011.
603 Targeting Acyl-CoA:diacylglycerol acyltransferase 1 (DGAT1) with small molecule
604 inhibitors for the treatment of metabolic diseases. The Journal of biological chemistry
605 **286:**41838-41851.
606 41. **Zechner R, Zimmermann R, Eichmann TO, Kohlwein SD, Haemmerle G, Lass A,**
607 **Madeo F.** 2012. FAT SIGNALS--lipases and lipolysis in lipid metabolism and signaling.
608 Cell Metabolism **15:**279-291.
609 42. **Manna PR, Cohen-Tannoudji J, Counis R, Garner CW, Huhtaniemi I, Kraemer**
610 **FB, Stocco DM.** 2013. Mechanisms of action of hormone-sensitive lipase in mouse
611 Leydig cells: its role in the regulation of the steroidogenic acute regulatory protein. The
612 Journal of Biological Chemistry **288:**8505-8518.
613 43. **Mayer N, Schweiger M, Romauch M, Grabner GF, Eichmann TO, Fuchs E, Ivkovic**
614 **J, Heier C, Mrak I, Lass A, Hofler G, Fledelius C, Zechner R, Zimmermann R,**
615 **Breinbauer R.** 2013. Development of small-molecule inhibitors targeting adipose
616 triglyceride lipase. Nature chemical biology **9:**785-787.
617 44. **Xu G, Sztalryd C, Lu X, Tansey JT, Gan J, Dorward H, Kimmel AR, Londos C.**
618 2005. Post-translational regulation of adipose differentiation-related protein by the
619 ubiquitin/proteasome pathway. The Journal of Biological Chemistry **280:**42841-42847.
620 45. **Newton HJ, McDonough JA, Roy CR.** 2013. Effector protein translocation by the
621 *Coxiella burnetii* Dot/Icm type IV secretion system requires endocytic maturation of the
622 pathogen-occupied vacuole. PLoS One **8:**e54566.
623 46. **Long AP, Manneschmidt AK, VerBrugge B, Dortch MR, Minkin SC, Prater KE,**
624 **Biggerstaff JP, Dunlap JR, Dalhaimer P.** 2012. Lipid droplet *de novo* formation and
625 fission are linked to the cell cycle in fission yeast. Traffic **13:**705-714.
626 47. **Paul A, Chang BH, Li L, Yechoor VK, Chan L.** 2008. Deficiency of adipose
627 differentiation-related protein impairs foam cell formation and protects against
628 atherosclerosis. Circulation Research **102:**1492-1501.
629 48. **Bozza PT, Payne JL, Morham SG, Langenbach R, Smithies O, Weller PF.** 1996.
630 Leukocyte lipid body formation and eicosanoid generation: cyclooxygenase-independent
631 inhibition by aspirin. PNAS **93:**11091-11096.
632 49. **Vieira-de-Abreu A, Calheiros AS, Mesquita-Santos FP, Magalhaes ES, Mourao-Sa**
633 **D, Castro-Faria-Neto HC, Bozza MT, Bandeira-Melo C, Bozza PT.** 2011. Cross-talk
634 between macrophage migration inhibitory factor and eotaxin in allergic eosinophil
635 activation forms leukotriene C(4)-synthesizing lipid bodies. American Journal of
636 Respiratory Cell and Molecular Biology **44:**509-516.
637 50. **Cao F, Castrillo A, Tontonoz P, Re F, Byrne GI.** 2007. *Chlamydia pneumoniae*--
638 induced macrophage foam cell formation is mediated by Toll-like receptor 2. Infection
639 and Immunity **75:**753-759.
640 51. **Deb C, Daniel J, Sirakova TD, Abomoelak B, Dubey VS, Kolattukudy PE.** 2006. A
641 novel lipase belonging to the hormone-sensitive lipase family induced under starvation to

642 utilize stored triacylglycerol in *Mycobacterium tuberculosis*. The Journal of biological
643 chemistry **281:**3866-3875.
644 52. **Dvorak AM, Dvorak HF, Peters SP, Shulman ES, MacGlashan DW, Jr., Pyne K,**
645 **Harvey VS, Galli SJ, Lichtenstein LM.** 1983. Lipid bodies: cytoplasmic organelles
646 important to arachidonate metabolism in macrophages and mast cells. Journal of
647 Immunology **131:**2965-2976.
648 53. **Weller PF, Monahan-Earley RA, Dvorak HF, Dvorak AM.** 1991. Cytoplasmic lipid
649 bodies of human eosinophils. Subcellular isolation and analysis of arachidonate
650 incorporation. The American journal of pathology **138:**141-148.
651 54. **Mattos KA, Oliveira VG, D'Avila H, Rodrigues LS, Pinheiro RO, Sarno EN,**
652 **Pessolani MC, Bozza PT.** 2011. TLR6-driven lipid droplets in *Mycobacterium leprae*-
653 infected Schwann cells: immunoinflammatory platforms associated with bacterial
654 persistence. Journal of Immunology **187:**2548-2558.
655 55. **Shannon JG, Heinzen RA.** 2009. Adaptive immunity to the obligate intracellular
656 pathogen *Coxiella burnetii*. Immunologic Research **43:**138-148.
657 56. **Koster FT, Williams JC, Goodwin JS.** 1985. Cellular immunity in Q fever: modulation
658 of responsiveness by a suppressor T cell-monocyte circuit. Journal of Immunology
659 **135:**1067-1072.
660 57. **Izzo AA, Marmion BP.** 1993. Variation in interferon-gamma responses to *Coxiella*
661 *burnetii* antigens with lymphocytes from vaccinated or naturally infected subjects.
662 Clinical and Experimental Immunology **94:**507-515.
663 58. **Cockrell DC, Beare PA, Fischer ER, Howe D, Heinzen RA.** 2008. A method for
664 purifying obligate intracellular *Coxiella burnetii* that employs digitonin lysis of host cells.
665 Journal of Microbiological Methods **72:**321-325.
666 59. **Omsland A, Cockrell DC, Howe D, Fischer ER, Virtaneva K, Sturdevant DE,**
667 **Porcella SF, Heinzen RA.** 2009. Host cell-free growth of the Q fever bacterium *Coxiella*
668 *burnetii*. Proceedings of the National Academy of Sciences of the U S A **106:**4430-4434.
669 60. **Sanjana NE, Shalem O, Zhang F.** 2014. Improved vectors and genome-wide libraries
670 for CRISPR screening. Nature Methods **11:**783-784.
671 61. **Coleman SA, Fischer ER, Howe D, Mead DJ, Heinzen RA.** 2004. Temporal analysis
672 of *Coxiella burnetii* morphological differentiation. The Journal of Bacteriology
673 **186:**7344-7352.
674

Figure 1

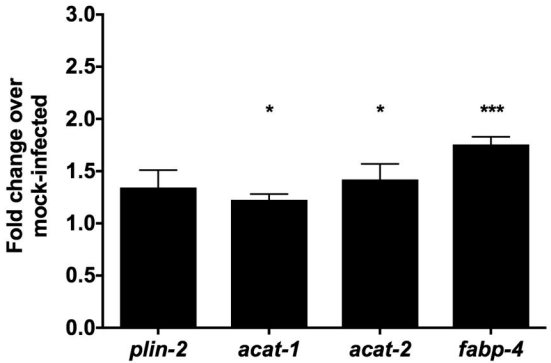

Figure 1: LD-associated genes are upregulated in *C. burnetii*-infected alveolar macrophages.
MH-S macrophages were infected with wild-type *C. burnetii* and RNA was collected at day 1 post-infection. Gene expression analysis was performed using Applied Biosystems lipid-regulated TaqMan Array. Fold change was calculated compared to mock-infected samples. Error bars show the mean of 6 independent experiments +/- SEM * =p<0.05, *** =p <0.001 compared to respective mock-infected cells as determined by two-tailed paired t-test.

Figure 2

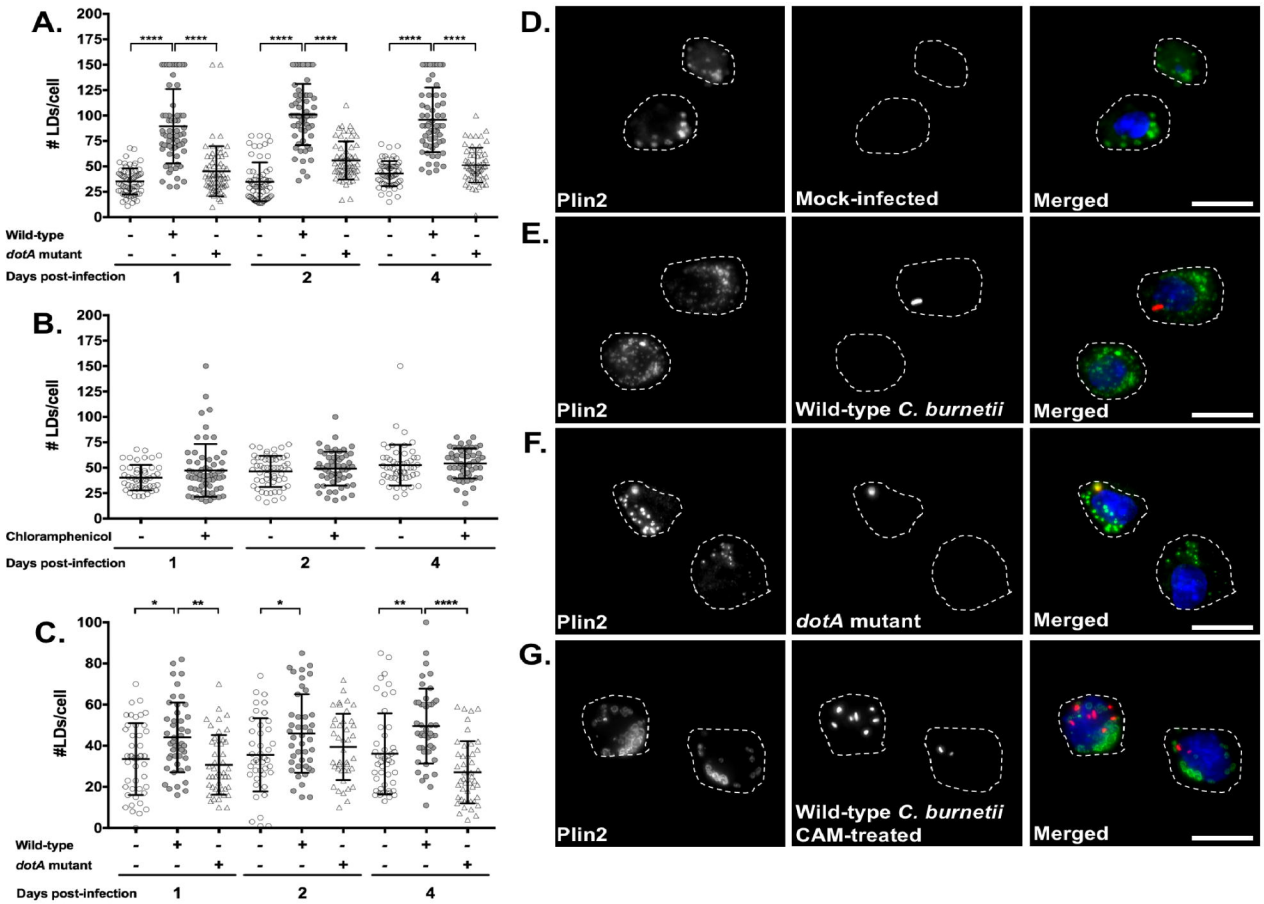

Figure 2: *C. burnetii* infection leads to host cell LD accumulation and is dependent on bacterial protein synthesis and the T4BSS.

Macrophages were infected with *C. burnetii* and at different times post-infection, cells were stained for PLIN2 (LDs; green), *C. burnetii* (red) and nucleus (blue). LD number per cell were quantitated by fluorescence microscopy.

A) LD numbers in wild-type *C. burnetii* and *dotA* mutant- infected MH-S macrophages.

B) LD numbers in MH-S macrophages infected with wild-type *C. burnetii* and treated with chloramphenicol (3ug/ml).

C) LD numbers in wild-type *C. burnetii* and *dotA* mutant- infected THP-1 macrophage-like cells.

D) Images of LDs and bacteria in MH-S cells at day 1 post-infection imaged at 100X. Scale bar = 10 µm. Error bars show the mean of 3 independent experiments +/- SEM * =p<0.05, ** =p <0.01, *** =p <0.001 as determined by ordinary one-way ANOVA with Tukey post-hoc test.

Figure 3

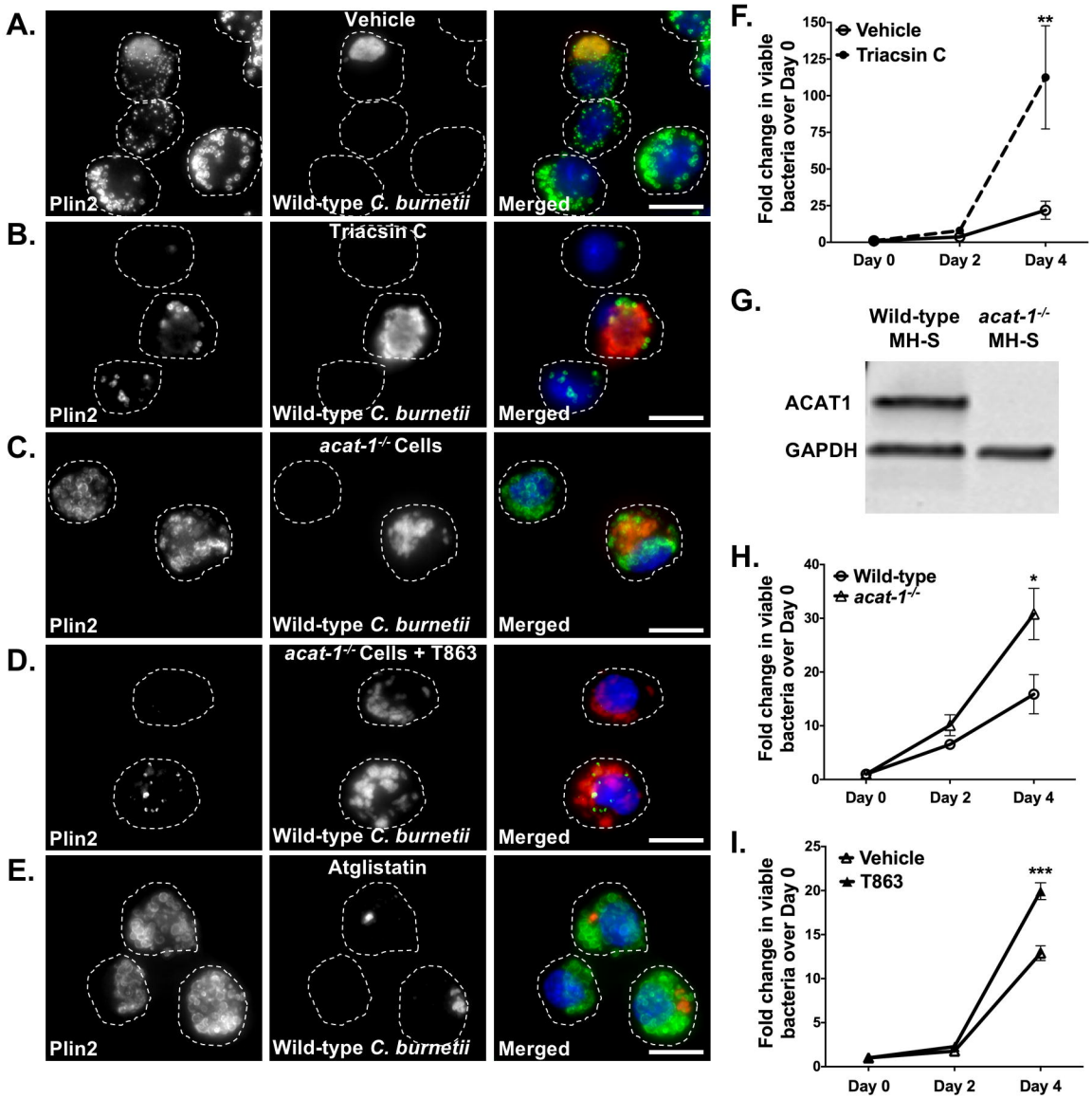

Figure 3: Blocking LD formation increases *C. burnetii* growth.
Wild-type *C. burnetii* growth in infected MH-S cells treated with different inhibitors was measured at 2 and 4 days post-infection by FFU assay.
A-E) Representative images for wild-type MH-S macrophages treated with inhibitors, fixed, stained for PLIN2 (LDs; green) and *C. burnetii* (red) and imaged day 4 post-treatment at 100X. Scale bar = 10 µm.
F) Growth while inhibiting LD formation with triacsin C (10 µM) in wild-type MH-S macrophages. Error bars represent the mean of 4 independent experiments +/- SEM. **= $p < 0.01$ compared to vehicle-treated cells as determined by two-way ANOVA with Bonferroni post-hoc test.
G) ACAT1 protein expression in wild-type and *acat-1*$^{-/-}$ macrophages. Cell lysates were immunoblotted and ACAT1 protein levels were compared with GAPDH as loading control.
H) *C. burnetii* growth in vehicle-treated wild-type and *acat-1*$^{-/-}$ MH-S macrophages and (I) T863-treated *acat-1*$^{-/-}$ MH-S macrophages. Error bars represent the mean of at least 3 independent experiments +/- SEM., * =$p<0.05$, *** =$p < 0.001$ as determined by two-way ANOVA with Bonferroni post-hoc test.

Figure 4

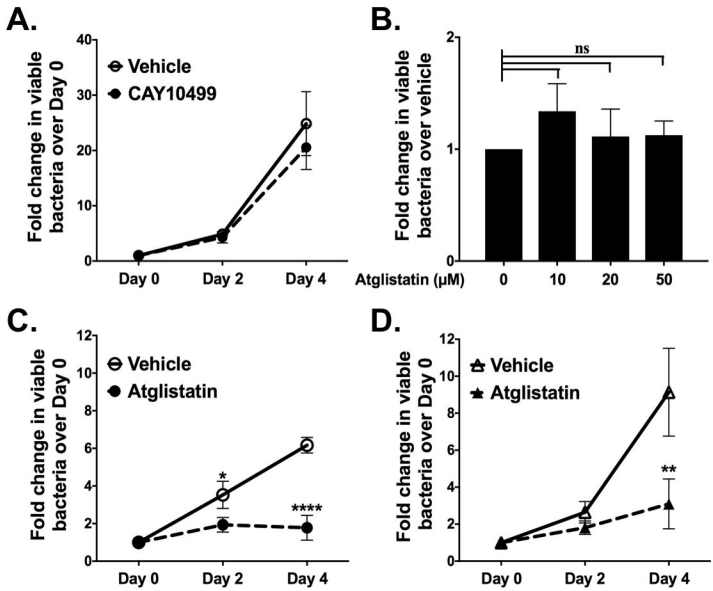

Figure 4: Inhibiting LD breakdown blocks *C. burnetii* growth.
Effect of HSL inhibitor CAY10499 and ATGL inhibitor atglistatin on viability of axenic and intracellular wild-type *C. burnetii* was determined by FFU assay.
A) *C. burnetii* growth in CAY10499-treated (10 μM) and vehicle-treated wild-type MH-S macrophages. Error bars represent the mean of 3 independent experiments +/- SEM. ns = not significant compared to vehicle-treated cells as determined by two-way ANOVA with Bonferroni post-hoc test.
B) Direct effect of atglistatin on wild-type *C. burnetii*. Atglistatin was added to axenic *C. burnetii* cultures and bacterial viability was determined at day 4 using FFU assay. Error bars represent the mean of 3 independent experiments +/- SEM. ns = not significant compared to vehicle treatment as determined by ordinary one -way ANOVA with Tukey post-hoc test.
C) *C. burnetii* growth in atglistatin-treated (20 μM) and vehicle-treated wild-type MH-S macrophages. Error bars represent the mean of 4 independent experiments +/- SEM. *= $p < 0.05$, ****= $p < 0.0001$ compared to vehicle-treated cells as determined by two-way ANOVA with Bonferroni post-hoc test.
D) *C. burnetii* growth in atglistatin-treated (20 μM) and vehicle-treated *acat-1*$^{-/-}$ MH-S macrophages. Error bars represent the mean of 4 independent experiments +/- SEM. **= $p < 0.01$ compared to vehicle-treated cells as determined by two-way ANOVA with Bonferroni post-hoc test.